

Magnetic flux participation in solar surface magnetism during solar cycle 24

Chun-Lan Jin and Jing-Xiu Wang

Key Laboratory of Solar Activity, National Astronomical Observatories, Chinese Academy of Sciences, Beijing 100101, China; cljin@nao.cas.cn

Received 2018 September 5; accepted 2018 November 15

Abstract This study aims at investigating surface magnetic flux participation among different types of magnetic features during solar cycle 24. State-of-the-art observations from *SDO/HMI* and *Hinode/SOT* are combined to form a unique database in the interval from April 2010 to October 2015. Unlike previous studies, the statistics presented in this paper are feature-detection-based. More than 20 million magnetic features with relatively large scale, such as sunspot/pore, enhanced and quiet networks, are automatically detected and categorized from HMI observations, and the internetwork features are identified from SOT/SP observations. The total flux from these magnetic features reaches 5.9×10^{22} Mx during solar minimum and 2.4×10^{23} Mx in solar maximum. Flux occupation from the sunspot/pore region is 29% in solar maximum. Enhanced and quiet networks contribute 18% and 21% flux during the solar minimum, and 50% and 9% flux in the solar maximum respectively. The internetwork field contributes over 55% of flux in the solar minimum, and its flux contribution exceeds that of sunspot/pore features in the solar maximum. During the solar active condition, the sunspot field increases its area but keeps constant flux density of about 150 G, while the enhanced network follows the sunspot number variation showing increasing flux density and area, but the quiet network displays decreasing area and somewhat increasing flux density of about 6%. The origin of the quiet network is not known exactly, but is suggestive of representing the interplay between mean-field and local dynamos. The source, magnitude and possible importance of ‘hidden flux’ are discussed in some detail.

Key words: Sun: magnetic fields — Sun: dynamo — Sun: photosphere — sunspots

1 INTRODUCTION

The term of solar cycle refers to a quasi-periodic variation with a period of about 11 years, visible in many aspects of the Sun’s observables. The easiest and earliest definition of solar cycle refers to the sunspot number changes. Sunspots are a manifestation of the Sun’s strong magnetic field. It is currently believed that the Sun operates an internal dynamo to generate, sustain and organize magnetic fields. The mean-field dynamo model (Moffatt 1978; Van Kampen 1976) is commonly accepted to interpret the origin and evolution of the solar general magnetic field, i.e., the magnetic field in the active belts and poles. However, the detailed flux emergence and evolution in solar active regions, and the rich observations of flux appearance and disappearance in the form of network and internetwork fields, are beyond the scope of the mean-field dynamo.

Solar magnetic fields are structured and organized in a hierarchy of spatial scales from hundreds of arcsec (i.e., sunspot magnetic field) to tens of arcsec (i.e., network field) and a few arcsec and even sub-arcsec (i.e., internetwork field and ‘hidden’ component). These magnetic structures account for the Sun’s total magnetic flux. Zhang et al. (2010) analyzed the active region in solar cycle 23, and found that the maximum flux of an individual active region would reach 1.97×10^{23} Mx. During solar maximum, the active regions contribute about 8×10^{23} Mx to the Sun (Schrijver & Harvey 1994). Similar to emerging flux regions (Zirin 1972) in sunspot groups, small-scale emerging bipoles named ephemeral regions were described by Harvey & Martin (1973). Furthermore, the flux emergence rate of ephemeral region turns out to be about 7.2×10^{22} Mx per day, and the ephemeral region and debris

of decaying active region explain the flux of the network (Schrijver et al. 1997). However, Gošić et al. (2014) found that the observed rate of internetwork flux transferring to the network was 1.5×10^{24} Mx per day over the entire solar surface, and 40% of the total internetwork flux eventually ended up in the network. The total flux that is emerging in internetwork elements exceeds that in the ephemeral region by two orders of magnitude and that in sunspot by four orders of magnitude (Zirin 1987). Wang et al. (1995) reported that internetwork magnetic elements contributed a total flux of 10^{23} Mx on the Sun, and more than 20% of the total flux in the quiet region was in the form of internetwork elements at any given time based on the Big Bear deep magnetogram. Lites (2002) indicated that internetwork flux contribution was larger than the 20% lower limit identified by Wang et al. (1995). Meunier et al. (1998) found that approximately 2/3 of the flux was in weak-field form in the quiet Sun. Based on the improved instrument of Solar Optical Telescope /Filtergraph (SOT/FG), Zhou et al. (2013) further analyzed the internetwork flux contribution, and concluded that a total of 3.8×10^{26} Mx flux on the quiet Sun would appear in a day and disappear in the form of internetwork elements, and 52% of the total flux in the quiet Sun came from the internetwork field.

Some fundamental questions are presented in solar magnetism such as how much each magnetic component contributes to the total solar magnetic flux at any given time in a solar cycle, and how much the flux occupation of each component is, and whether or not the flux occupation changes in a sunspot cycle. Further, how much area is still undetectable in the state-of-the-art polarization measurements? In this study, we aim to get a quantitative idea about the participation of each component in solar magnetism and its changes in a solar cycle, and give further hints and constraints on understanding the origin of the solar magnetic field. The full-disc magnetic observations from Helioseismic and Magnetic Imager (HMI: Scherrer et al. 2012; Schou et al. 2012) and the highly accurate polarimetric observations from SOT/Spectro-Polarimeter (SOT/SP: Tsuneta et al. 2008; Suematsu et al. 2008; Ichimoto et al. 2008; Shimizu et al. 2008) provide a chance for us to work on this study. This paper is organized as follows. Section 2 is devoted to the data observations and analysis. We present the observed categories in solar surface magnetism of HMI observations in Section 3. In Section 4 we analyze flux participation and occupation. In Section 5 we discuss the hidden magnetic flux and in Section 6 we give concluding remarks and discussion.

2 DATA OBSERVATIONS AND ANALYSIS

2.1 HMI Observations

The HMI instrument is filtergraph-based with full-disk coverage of 4096×4096 pixels. Its spatial resolution is 1 arcsec with a 0.5 arcsec pixel size (Schou et al. 2012). The spectral line FeI 6173 Å in the photosphere is adopted to obtain the line-of-sight magnetic field. Such a full-disk magnetogram is acquired with a cadence of 45 seconds. Since April 2010, HMI has provided round-the-clock full-disk magnetic measurements.

The magnetogram observations in an interval from April 2010 to October 2015 are taken in this study, and 2010 sets of magnetograms are used. Considering the limb-weakening of line-of-sight field (e.g., Jin & Wang 2011), in this study we assume that the magnetic field (B_{in}) is radial, and the observed line-of-sight field (B_{los}) is a projection of B_{in} in the line-of-sight direction (Hagenaar 2001; Jin et al. 2011). In this study, the magnetic field refers to the flux density per pixel. There is some unreasonable aspect of the radial assumption, especially for the weak field. However, the method indeed removes the limb-weakening of line-of-sight field in some sense. We correct the full-disk magnetic field by $B_{in} = B_{los} / \cos(\alpha)$, where α is defined by $\sin(\alpha) = \sqrt{(x^2 + y^2)} / R$, x and y are the pixel position referring to disk center, and R is the radius of the Sun. According to the magnetic correction $1/\cos(\alpha)$, the magnetic noise level would increase with positions far away from solar disk center, so we consider only these pixels for which $\alpha \leq 60^\circ$. The magnetic field of these pixels with $\alpha > 60^\circ$ is set to zero and not considered. In addition, the foreshortening effect of the pixel area is also corrected.

In order to improve the signal-to-noise ratio (S/N), we average the magnetic observations of seven continuous magnetograms in an interval of five minutes to create a 5-min average magnetogram. Then, for these 5-min average magnetograms, following the method of estimating noise level (Hagenaar 2001; Liu et al. 2004; Jin et al. 2011) we analyze the histogram of full-disk magnetic field, and assume that the magnetic field has a Gaussian distribution. Finally, we fit the distribution of the low-field pixels from the magnetograms by using a Gaussian function, and define the half-width of the Gaussian function as 1σ . The black dashed line in the top panel of Figure 1 indicates the distribution of magnetic field for 5-min average magnetograms, and red dotted line shows the Gaussian function fitting of the magnetic distribution. The half-width of the Gaussian function is 2.6 G. Here, $\sigma = 3$ G is adopted in this

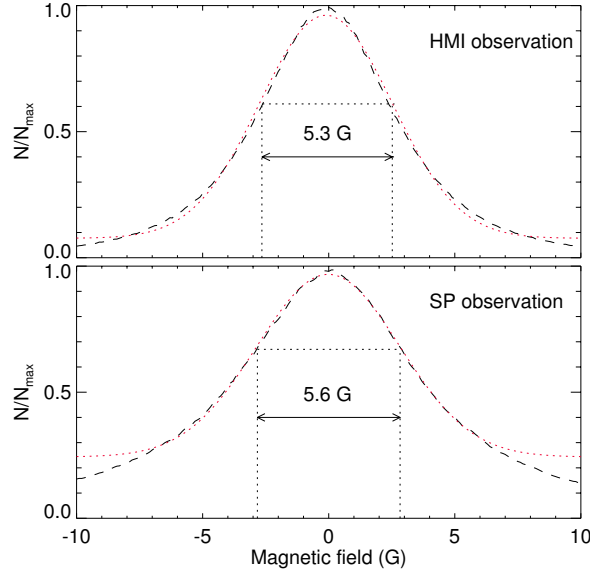


Fig. 1 Distribution function of magnetic field in the 5-min HMI magnetogram and SP observation. The *red dotted curve* shows a Gaussian fit to the core of the distribution function. The *black dotted lines* indicate the full-width 2σ .

study. Regarding the long-term stability of the HMI data, we analyze the change of the half-width of the corresponding Gaussian distribution for the entire interval. The result is given in Figure 2, showing that the 1σ value remains nearly unchanged, which can be set as 2.7 G throughout.

2.2 SOT/SP Observations

SOT/SP is a spectrograph-based instrument that records Stokes line profiles of two magnetically sensitive FeII lines at 6301.5 Å and 6302.5 Å and the nearby continuum. The SOT/SP mainly adopts four modes of operation with different polarimetric S/N and pixel size, i.e., Dynamics, Fast Map, Normal Map and Deep Magnetogram. In this study, we choose the Normal Map mode observation with large field-of-view. Table 1 shows the used database. The observation mode produces polarimetric accuracy of 0.1% with $0.15'' \times 0.16''$ pixel size (Tsuneta et al. 2008). It takes about 150 minutes to scan a 260 arcsec-wide area. In order to extract as many weak magnetic signals as possible, the wavelength-integrated method is adopted to obtain the magnetic field as described by Lites et al. (2008). The wavelength-integrated Stokes V is defined as

$$V_{\text{tot}} = \text{sign}(V_{\text{blue}}) \frac{|\int_{\lambda_b}^{\lambda_0} V(\lambda) d\lambda| + |\int_{\lambda_0}^{\lambda_r} V(\lambda) d\lambda|}{I_c \int_{\lambda_b}^{\lambda_r} d\lambda}, \quad (1)$$

where $\text{sign}(V_{\text{blue}})$ means the sign of the blue peak of the Stokes V profile, λ_0 represents the wavelength of Stokes V zero-cross, and λ_r and λ_b signify the limits of integration for the spectral line.

We select some magnetic structures simultaneously observed by SOT/SP and HMI, and then consistently calibrate the magnetic field of HMI and SP magnetograms. The result is displayed in the left panel of Figure 3, and the red solid line indicates the linear fit between two measurements. It can be found that the magnetic flux density derived from SP data is greater than that inferred from HMI data by a factor of 1.18. In this study, the magnetic field in SP magnetograms is divided by a factor 1.18 to match that of the HMI observations.

We also adopt the Gaussian distribution method to estimate the 1σ of SOT/SP magnetic observation, which is shown in the bottom panel of Figure 1. The half-width of the Gaussian function is 2.8 G. In this study, $\sigma = 3$ G is adopted.

2.3 Comparison between HMI Magnetograms and SOT/SP Measurements

The spatial resolution and polarization sensitivity of the magnetograph set the detectability limit in magnetic observations. Therefore, different systems are detecting somewhat different magnetic components. A comparison of observations between two instruments is necessary in order to clarify which magnetic components are being observed. There is no doubt that the ubiquitous internetwork fields can be detected based on the SOT/SP observations (Lites et al. 2008). In order to understand very well which components are being observed by HMI measurement, here we

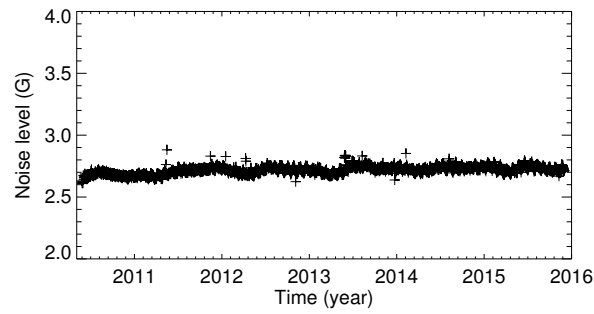


Fig. 2 Time profile of the half-width of Gaussian fitting for distribution function of weak field observed daily with HMI from April 2010 to October 2015.

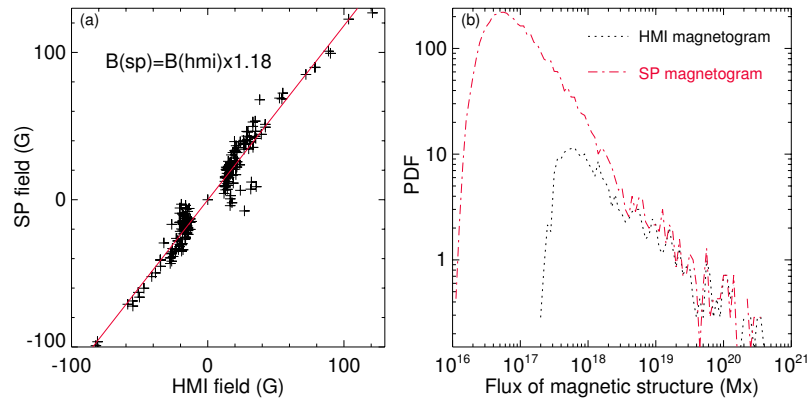


Fig. 3 *Left panel*: the magnetic calibration between HMI and SP magnetograms. *Right panel*: the flux distribution comparison for magnetic structures identified in HMI and SP observations.

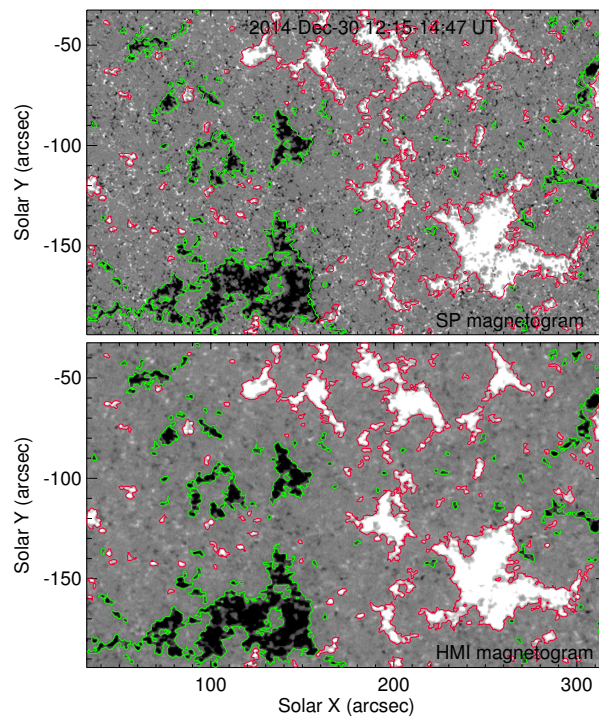


Fig. 4 The comparison of HMI and SP magnetograms. The HMI magnetogram is reconstructed in the interval where the SP magnetogram is scanned. The regions contoured by *green* and *red* lines mean the magnetic structures identified by the HMI observations.

make the comparison of magnetograms taken by HMI and SP.

We align the SP and HMI magnetograms in both spatial and temporal domains. Firstly, we choose and download all HMI magnetic observations in the interval of the scanning SP magnetogram, and then average these HMI observations in a 5-min interval. Secondly, we extract the HMI observations with the same region as the SP observation, and then construct a slit-scanning map from the time series of HMI magnetograms. Figure 4 shows the aligned SP and constructed HMI magnetograms. The green and red contour lines represent the magnetic structures identified by HMI observation. From the figure, we find that in the apparent unknown region of HMI, the internetwork field is clearly exhibited by the SP observation, as described by Lites et al. (2008). It suggests that the HMI observation does not have the capability to detect the internetwork field.

Then for the SP and reconstructed HMI magnetograms, we identify their magnetic structures based on a magnetic threshold of 3σ and an area threshold of 3×3 pixels (i.e., an area of $0.45'' \times 0.48''$ for SP and $1.5'' \times 1.5''$ for HMI). The histogram of flux distribution is represented by the black dotted line for HMI observation and the red dash-dotted line for SP observation in the right panel of Figure 3. From the figure, it can be ascertained that comparing the flux distribution of the internetwork field with a peak distribution at $(5 - 6) \times 10^{16}$ Mx, HMI observations show a peak flux distribution at 6×10^{17} Mx. It is interesting to note that the peak flux distribution of the internetwork field identified from SOT/SP coincides with that revealed from the long-integrated magnetograms of ground-based instrumentation (Wang et al. 1995).

3 OBSERVED CATEGORIES IN SOLAR SURFACE MAGNETISM OF HMI OBSERVATION

In this study, the observed categories of magnetic field are based on the identification of magnetic structures in solar magnetograms by considering their area and magnetic field. For each 5-min average and corrected HMI magnetogram, we apply a magnetic field of 3σ and an area of 3×3 pixels as the thresholds to extract magnetic structures and then create a mask for each magnetogram. These regions of identified magnetic structures are thought to be the magnetic signal regions, and the remanent regions in the magnetogram are defined as the ‘unknown region’ in this study.

For these pre-conducted 5-min HMI magnetograms, we totally extract more than twenty million magnetic structures in the 2010 sets of magnetograms that were obtained in the interval from April 2010 to October 2015. Indeed, we introduce observational categories from the flux distribution. Magnetic flux distribution presents an independent perspective for gaining an understanding of each ingredient in solar radiation and activity. There is no doubt about what sunspots and pores are from continuum intensity imaging. Firstly, we strictly extract sunspot/pore magnetic structures by comparing magnetic features with continuum intensity. We examine large samples, and choose the following working definition on sunspot/pore structures in 5-min HMI magnetograms: when the magnetic flux of a magnetic structure is larger than 1.0×10^{20} Mx and its maximum magnetic field is larger than 950 G, we define the magnetic structure as a sunspot/pore structure. By this criterion, the sunspot/pore structures are basically extracted in HMI magnetograms, and two samples of identified sunspot and pore are shown in Figure 5.

Secondly, the remanent magnetic structures, i.e., excluding sunspot/pore features, in these magnetograms range in their flux from the detection limit of HMI observations (i.e., 10^{17} Mx) to about 10^{20} Mx. It is difficult to distinguish these magnetic structures by magnetic features and continuum intensity. However, they display obviously different radiations in the chromosphere. Just as described in Section 2.3, HMI observation cannot detect the internetwork structures, so in this study, we divide these structures into two categories: quiet and enhanced networks. The term of enhanced network was introduced in solar physics in the 1970s (e.g., Marsh 1977; Gaizauskas 1979; and until the recent work by Carlsson et al. 2016). Compared with quiet network, enhanced network is characterized by a relatively strong magnetic field and obvious brightening in the chromosphere. We examine large samples by considering magnetograms and central line CaII images, and the enhanced and quiet networks are distinguished by the following criteria: when the magnetic flux of a magnetic structure is larger than 7.0×10^{18} Mx and its maximum magnetic field is larger than 100 G, we define the magnetic structure as an enhanced network, which is shown by the green lines in Figure 6; the other remanent magnetic structures are categorized as quiet networks. From this figure, it can be found that enhanced networks basically include those magnetic structures with obviously bright features. Further, we analyze the flux variations for quiet and enhanced networks, and compute the correlated coefficients

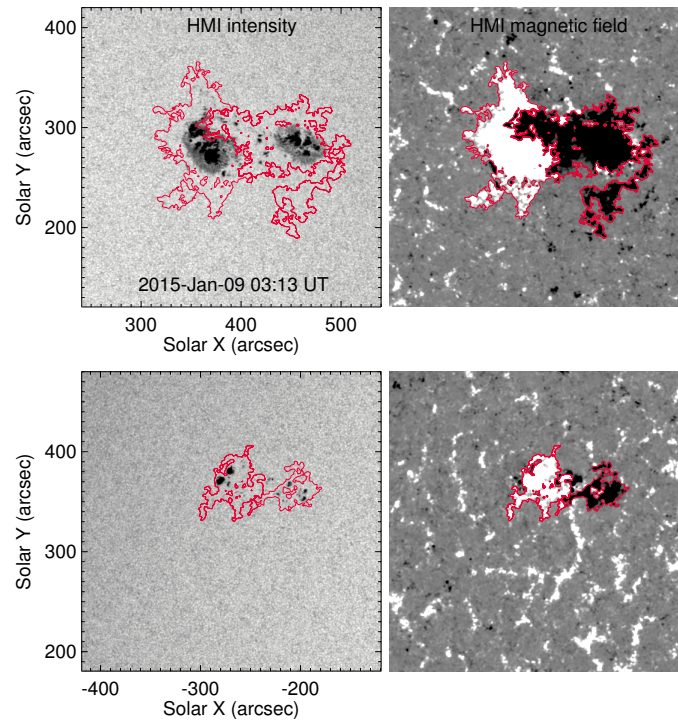


Fig. 5 The extraction of sunspot/pore based on the criterion of flux threshold 1.0×10^{20} Mx and maximum magnetic field of 950 G. The regions shown by *red lines* are the identified sunspot and pore.

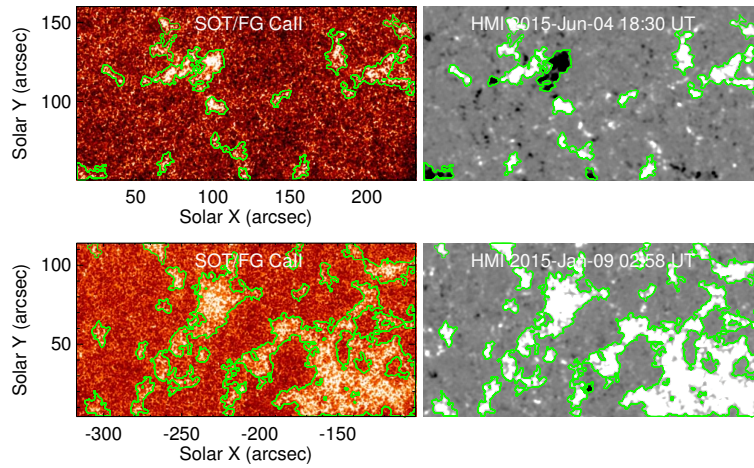


Fig. 6 The extraction of enhanced network based on the criterion of flux threshold 7.0×10^{18} Mx and maximum magnetic field of 100 G in the magnetogram, excluding sunspot/pore. The regions shown by the *green lines* are the identified enhanced network.

between their flux variations and sunspot cycle. It can be found that the coefficients are 0.81 for enhanced networks and -0.21 for quiet networks. The results mean that the enhanced and quiet networks are showing different cyclic variations.

As an examination, we divide these magnetic structures excluding sunspot/pore features into 61 sub-groups according to their flux magnitude, and create a statistical sample of magnetic structures covering the flux range from the detection limit of HMI (1.7×10^{17} Mx) to 10^{20} Mx.

The monthly flux variation of magnetic structures for each sub-group is analyzed, and the correlation coefficients between the variations of magnetic flux for each sub-group and sunspot numbers are computed. The result is shown in Figure 7. We can find that, within a small range above the detection limit of magnetic flux by HMI (up to 5.8×10^{18} Mx), the flux of the magnetic structures exhibits a negative correlation with sunspot cycle. The negative correlation becomes weaker when the magnetic flux of the chosen range increases. When the flux becomes larger than

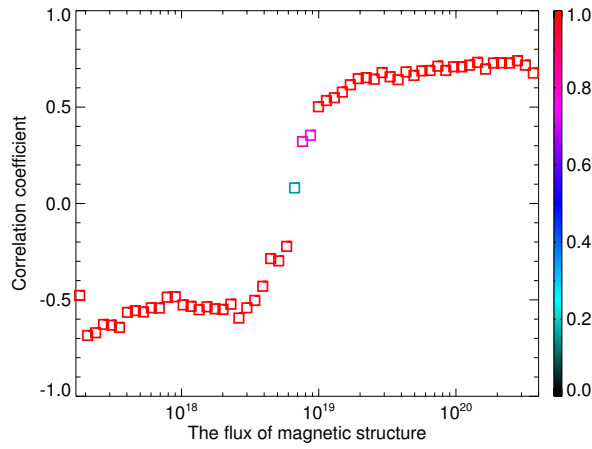


Fig. 7 The correlation coefficient between sunspot cycle and network flux spectrum variation. The network flux is obtained by detecting magnetic structures excluding sunspot/pore based on HMI long-term observations. From the detection limit to the large flux spectrum, the flux of magnetic structures shows anti-phased and in-phased variation with sunspot cycle. The right color-bar tells the confidence level.

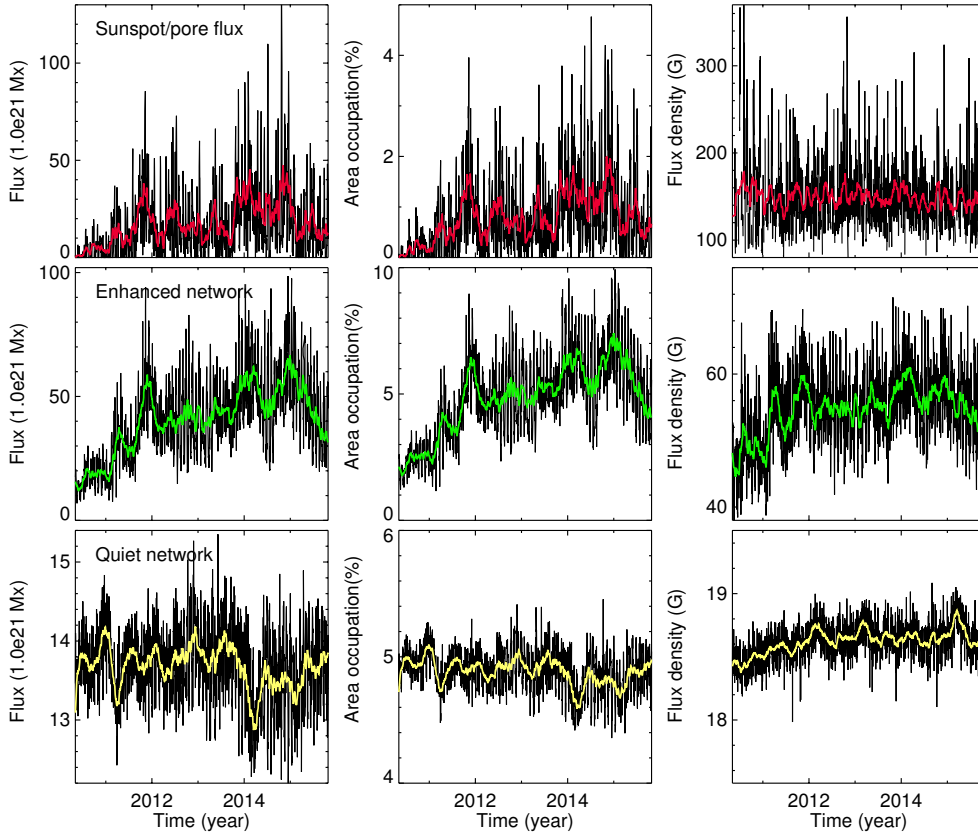


Fig. 8 The variations of magnetic flux, area occupation and flux density for different magnetic components based on HMI observations. The colored line in each panel means the corresponding 30-day smoothing.

7.0×10^{18} Mx, the correlation switches to be positive, with the correlation coefficient increasing with increasing flux until the flux is larger than 2.0×10^{19} Mx when it keeps the value of about 0.75. The enhanced network represents the concentration of these in-phase magnetic structures, while the quiet network mainly includes these anti-phase

magnetic structures. In addition, the flux spectral variation confirms the conclusion from Jin et al. (2011) based on the analysis of MDI magnetograms, but different from the early work, and the transition flux from the positive correlation magnetic structures to anti-correlated magnetic structures shifts from $\sim 4 \times 10^{19}$ Mx (Jin et al. 2011) to

$\sim 6 \times 10^{18}$ Mx in this study. In a statistical sense, the reason for the transition flux shifting towards low flux is that some magnetic concentrations observed in MDI are clusters of magnetic structures in the HMI observation with higher spatial resolution.

The different behaviors of two types of network features correlated with sunspot cyclic variation demonstrates, on the other hand, that the categorization of enhanced and quiet networks is physically meaningful.

4 FLUX PARTICIPATION AND OCCUPATION

We study the cyclic variations of the daily magnetic flux, area and flux density for the sunspot/pore features, enhanced and quiet networks. The results are shown in Figure 8, and the colored line in each panel means the corresponding 30-day smoothing. From the figure, it can be found that the cyclic variation of magnetic flux carried by sunspots and pores, which is suggested to be produced by mean-field dynamo, results from its area change on the solar surface, while its flux density does not show a clear variation trend but maintains a median value of approximately 150 G in this period. We definitely cannot exclude the influence from the saturation effects for sunspot umbra from stray light and that in measuring sunspot/pore magnetic field based on the weak-field approximation method. We compute the ratio of the umbra area to the magnetic structure area of sunspot/pore, and find the ratio is very small, in the range from 0.9% to 8.8%. In addition, the average flux density for sunspot/pore magnetic structures is in the order of magnitude of hecto-Gauss based on the weak-field approximation measurements. The influence from the saturation effects is thought to be not important. For the enhanced networks, their flux increases from 6.8×10^{21} Mx at the beginning of HMI observation (i.e., early in the ascending phase of cycle 24) to 9.8×10^{22} Mx in solar maximum by a factor of 14. Furthermore, both their area and flux density increase in this period. That is to say, both the flux density variation and area variation from enhanced network follow the sunspot cycle. For the quiet networks, their flux decreases to 1.2×10^{22} Mx in solar maximum, which shows anti-correlated variation with sunspot cycle. However, the flux density from quiet networks somewhat displays increases of about 6% during solar active condition, that is to say, the anti-correlated variation of quiet network flux with sunspot comes from its area change.

However, even with the spatial resolution of HMI observations, there is still a big mass of region which is covered by the magnetic field below the detection limit. In

other words, a large amount of magnetic flux is likely to be hidden below the polarization sensitivity of HMI, including that which can be observed as internetwork field by SOT/SP. In this study, we quantitatively analyze the daily area occupation of HMI unknown region, and inspect its cyclic variation, which is shown in Figure 9. The colored line in the top and middle panels of Figure 9 traces the 30-day smoothing. We find that the area occupation of unknown region exceeds 93% in the solar minimum of cycle 24, and the area occupation decreases when solar activity increases. However, even in the solar maximum of cycle 24, the area ratio of unknown region still reaches about 83.5%. As cycle 24 is a particularly weak cycle, we are not able to say if the statistics would be valid for other solar cycles.

Comparing with the HMI magnetic observations, the SOT/SP instrument with higher spatial resolution and polarization sensitivity can detect smaller-scale magnetic structures, and these smaller-scale magnetic structures mainly represent the internetwork field. We select some regions observed by SOT/SP with a large field-of-view, i.e., over 100 arcsec in both coordinates. The database is listed in Table 1. We align the SP observation and HMI observation in the same spatial and temporal domains, which is described in detail in Section 2.3. In the HMI unknown region, we find that in about 16% – 19% of the area one still can detect magnetic signals based on the SP observations. Further, in these unknown regions of HMI magnetograms, we identify the internetwork magnetic structures by setting an area threshold of 3×3 pixels and magnetic threshold of 3σ based on SP observation, and then compute the magnetic flux in HMI defined unknown region and the magnetic flux of these internetwork magnetic structures by the SOT/SP observations in the same region. The result is shown in Table 2. It is found that the magnetic flux of internetwork structures from SP observation is comparable to the flux from HMI unknown region both in solar minimum and maximum. Hence, the internetwork flux magnitude of SOT/SP observations can be estimated by the flux value of HMI unknown region.

Moreover, we adopt a reasonable assumption that local information about the internetwork field can embody the global information, and combine the HMI and SOT/SP observations together. Therefore, the daily internetwork flux magnitude is shown in the middle panel of Figure 9. From the figure, it can be ascertained that at least 3.6×10^{22} Mx flux in the Sun is underestimated in the HMI unknown region compared with SOT/SP observations, even in the

Table 1 *Hinode* SOT/SP Images

Image	Observation time	Operation mode	Field-of-view (arcsec)	(X, Y) (arcsec)
1	2010 Dec. 12 11:04–12:31	Normal Map	148.8 × 163.8	(−2.7, 6.4)
2	2012 Feb. 16 14:53–16:19	Normal Map	151.4 × 163.8	(228.1, 145.4)
3	2012 Aug. 30 10:32–11:37	Normal Map	114.0 × 122.9	(249.7, 322.3)
4	2014 Dec. 01 10:08–12:40	Normal Map	262.5 × 163.8	(−176.3, −191.8)
5	2014 Dec. 30 09:37–12:10	Normal Map	265.8 × 163.8	(−106.6, −113.5)
6	2014 Dec. 30 12:15–14:47	Normal Map	263.7 × 163.8	(174.1, −113.3)
7	2015 Jan. 16 09:55–12:28	Normal Map	265.0 × 163.8	(−141.3, 250.9)
8	2015 Jan. 16 12:36–15:08	Normal Map	265.8 × 163.8	(139.9, 251.2)
9	2015 Jan. 17 10:30–13:02	Normal Map	265.0 × 163.8	(−141.3, −79.2)
10	2015 Jan. 25 10:01–12:32	Normal Map	260.9 × 163.8	(−141.7, 233.1)

Notes: Central position, X, Y arcsec of disk center.

Table 2 The Comparison of Flux Estimation of SP Data with HMI Data in HMI Unknown Region

Image	Date	HMI unknown region	SP signal region	r
1	2010 Dec. 12	4.21×10^{20} Mx	4.32×10^{20} Mx	16.36%
2	2012 Feb. 16	4.60×10^{20} Mx	4.58×10^{20} Mx	17.66%
3	2012 Aug. 30	2.76×10^{20} Mx	2.30×10^{20} Mx	18.30%
4	2014 Dec. 01	7.89×10^{20} Mx	7.99×10^{20} Mx	17.30%
5	2014 Dec. 30	7.57×10^{20} Mx	7.86×10^{20} Mx	16.63%
6	2014 Dec. 30	7.07×10^{20} Mx	6.92×10^{20} Mx	17.30%
7	2015 Jan. 16	8.30×10^{20} Mx	7.20×10^{20} Mx	16.83%
8	2015 Jan. 16	7.44×10^{20} Mx	7.67×10^{20} Mx	18.53%
9	2015 Jan. 17	7.13×10^{20} Mx	7.21×10^{20} Mx	16.99%
10	2015 Jan. 25	6.48×10^{20} Mx	6.44×10^{20} Mx	18.24%

Notes: The parameter r means the area ratio of internetwork signal region to internetwork region.

solar maximum. Accordingly, we adopt the full-disc HMI magnetic observation to study the magnetic components with larger scale (i.e., sunspot/pore, enhance and quiet networks), and adopt the comparison of SOT/SP and HMI observations to estimate the flux magnitude of the internetwork field. The flux occupation of sunspot/pore, enhanced network, quiet network and internetwork field is analyzed, which is shown in Figure 10. The colored lines display the 30-day smoothed flux occupation. We find that the flux occupation of sunspot/pore only reaches 29% of the total flux even in the solar maximum. The enhanced network contributes most flux in the solar maximum, reaching about 50%, while the quiet network only contributes about 9% of flux to the Sun in the solar maximum. Furthermore, in the solar minimum, flux occupation of internetwork field exceeds 55%, and the internetwork flux occupation is obviously larger than that of sunspot/pore even in the solar maximum.

5 A DISCUSSION ON HIDDEN MAGNETIC FLUX

In case a magnetic feature is distinguishable in the observation, like the cases described above, for simplicity the feature is assumed to have a Gaussian distribution in the magnetic field with the maximum field of B_{\max} and half-width a . Because of the effects of seeing and/or instrument, assuming again a Gaussian profile with half-width b , the feature would be observed as (see Wang et al. 1995)

$$B_{\text{obs}} = [a^2/(a^2 + b^2)]B_{\max} \exp[-\rho^2/(a^2 + b^2)], \quad (2)$$

where ρ is the radius in polar coordinates. The maximum magnetic field of the feature in an observation is reduced by a factor of $a^2/(a^2 + b^2)$, and the feature is enlarged to a maximum width of $(a^2 + b^2)^{1/2}$. However, the magnetograph has limited sensitivity, and it can only detect a magnetic field above B_d . Then a certain amount of flux becomes hidden in the observation, which is

$$\phi_{\text{hidden}} = \phi_{\text{real}}[(a^2 + b^2)/(\gamma \times a^2)], \quad (3)$$

where $\gamma = B_{\max}/B_d$. When $[(a^2 + b^2)/(\gamma \times a^2)] \geq 1$, all the flux of the feature is hidden. It would be interesting to

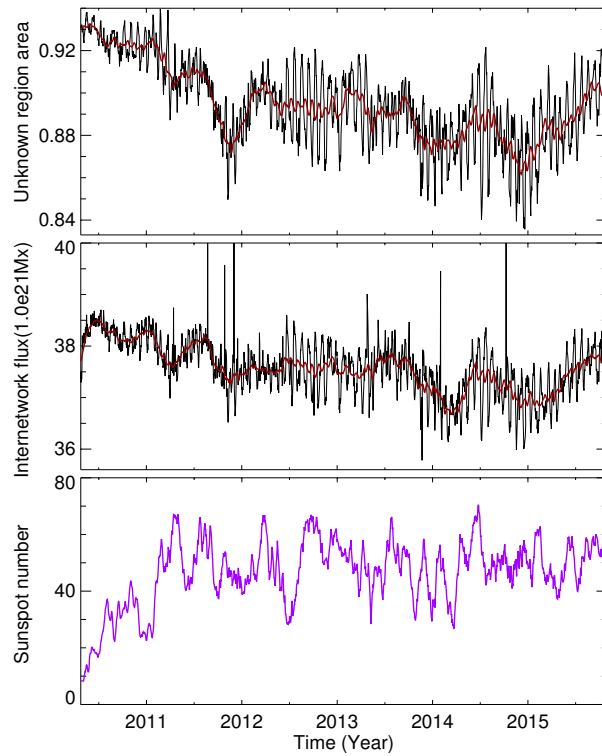


Fig. 9 The daily area variations for the unknown region based on HMI magnetic observation, the daily internetwork flux observation by combining HMI and SOT/SP observations, and the corresponding 30-day smoothing sunspot number in this period. The *brown lines* trace the 30-day smoothing of the corresponding parameters.

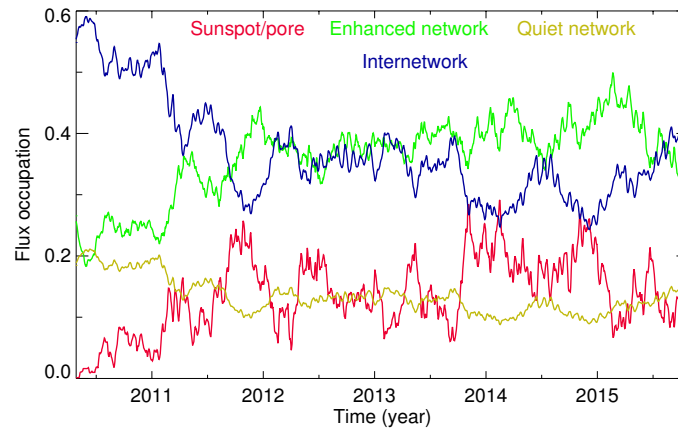


Fig. 10 The magnetic flux occupations of sunspot/pore (*red line*), enhanced network (*green line*), quiet network (*yellow line*) and internetwork field (*blue line*) based on the merged observations from HMI and SOT/SP.

look at the early solar observations, when B_d was not better than 20 G, and the seeing and instrument effects could not be smaller than $1''$. For a hecto-Gauss magnetic feature with $0.1''$ in half-width, there would be no flux being measured.

As for *Hinode* SOT/SP observations, the sensitivity is high with $1\sigma < 3$ G, and then one can take $B_d = 10$ G. For a hecto-Gauss magnetic feature, e.g., $B_{\max} = 300$ G, assuming $a = 0.1''$, the real flux of this magnetic feature

is 3.1×10^{16} Mx. When γ is about 30 and b is smaller than $0.3''$, the hidden flux will amount to 1/3 of the real flux, e.g., 1.0×10^{16} Mx. However, when the feature is larger, e.g., $a = 0.6''$ and $B_{\max} = 500$ G, the hidden flux becomes 2.5% of the real one. Since the sensitivity and spatial resolution have been largely improved in space-based observations, the hidden flux would not be as high as early ground-based observations. But, when considering the in-

ternetwork participation in the Sun's total flux, this type of hiding effect should be taken into account.

Referring to the above discussion, what one observed for a distinguishable magnetic feature in a magnetogram is the magnetic field inside a circle with radius

$$\rho_d = (a^2 + b^2)^{1/2} \ln[\gamma \times a^2 / (a^2 + b^2)]^{1/2}. \quad (4)$$

Outside the circle, the flux density becomes lower than the detection limit, therefore, the relevant flux is hidden. When $[\gamma \times a^2 / (a^2 + b^2)] < 1$, all the flux of the feature is hidden (Wang et al. 1995).

Things become more complicated if there are indistinguishable magnetic features with opposite polarities in a resolvable element of magnetograms. When seeing and/or instrument profiles are present, usually the algebraic sum cannot completely cancel the magnetic flux of opposite polarities. For simplicity, we assume two identical magnetic features with just opposite polarities, and they are separated by a distance of s . In a magnetogram we should observe the following flux distribution

$$B_{\text{obs}} = [a^2 / (a^2 + b^2)] B_{\text{max}} \exp[-\rho^2 / (a^2 + b^2)] \times [1 - \exp(s(2\rho - s) / (a^2 + b^2))]. \quad (5)$$

It is clear that when $s = 0$, $B_{\text{obs}} = 0$ always; and close to the position of $\rho = s/2$, $B_{\text{obs}} \approx 0$ too. For most cases, s is smaller than $2\rho_d$, and sometimes one might still be able to see the two magnetic features in the outskirts of the two smaller features with severely reduced flux. The algebraic summation of the two features' flux with opposite polarities seems to largely reduce the unsigned total flux, mostly in the internetwork domain or at further small scales. It is possible that the observed small flux fibers are the remains of such an algebraic summation.

Limited by the spatial resolution of state-of-the-art instruments, we are not able to detect magnetic features at very small scales. However, in case the magnetic structure numbers vary with magnetic flux by following the power law with index $\delta > 1$ (see Wang et al. 1995; Parnell et al. 2009; Zhou et al. 2013), we may write the frequency $N_f(\phi)$ of magnetic features with flux ϕ in the form $N(\phi) = N_f \phi^{-\delta}$. The total flux of all magnetic features can be estimated by an integration

$$\phi = \int_{\varphi_{\text{min}}}^{\varphi_{\text{max}}} N(\varphi) \varphi d\varphi. \quad (6)$$

As discussed by Parnell & Jupp (2000), referring also to early discussion by Hudson (1991), when $\delta < 2$, the total flux would be determined by the upper limit of the

integration. Considering the fact that magnetic flux in features with flux larger than 10^{16} Mx has been observationally measured, the hidden flux at the small-scale end can be estimated by

$$\phi_{\text{hid}} = \frac{A_{\text{Sun}} N_f}{2 - \delta} \varphi_{\text{max}}^{2-\delta}. \quad (7)$$

Here, we take $\varphi_{\text{max}} = 10^{16}$ Mx, $\delta = 1.85$ and $N_f = 3 \times 10^{-4} \text{ Mx}^{-1} \text{ cm}^{-2}$ by following Parnell et al. (2009), and A_{Sun} is the area of the Sun. The ϕ_{hid} is found to be approximately 5×10^{21} Mx. However, there is an uncertainty regarding the power-law flux distribution. Although within eight orders of magnitude in features' magnetic flux the power-law serves as a good approximation, the constant term N_f may only be valid piece by piece in the flux spectrum. We shall allow a variation of N_f by an order of magnitude or so (Zhou et al. 2013). Therefore, the hidden flux may fall in the range 10^{21} - 10^{22} Mx.

Almost 30 years ago, a solar astrophysicist commented on the eager demands for higher resolution in solar observations. He asked one of the current authors: when you reach $1''$ resolution, you want $0.1''$; while after that you ask for $0.01''$, and what is the end of the trial, 1 km or even 1 meter? (Biao Chen 1989, private communication). The question is penetrating. Justification from a certain scope of physics is unavoidable.

A relevant question here is how important the hidden flux would be in solar radiation and dynamics. Do we really need to be bothered by the hidden flux if it always happens on extremely small scales?

The solar magnetic field is three dimensional (3D). A concept in this regard is the anchor depth of various magnetic features from the solar surface. The concept was first introduced in solar physics by Javaraiah & Gokhale (1997). A careful approach was made by Sivaraman & Gokhale (2004). It is also necessary to know their extent into the solar atmosphere, since the energy carried by a magnetic feature is the integration of its volume and duration. How high the magnetic field is penetrating in the solar atmosphere would be critical to understanding solar activity and coronal heating.

Sivaraman & Gokhale (2004) estimate the anchor depths of the various surface magnetic features as the location of the Sun's internal plasma layers that have the same rotation rate as these magnetic features on the solar surface. They conclude that spot groups living 10 to 20 days are initially around the base of the convective zone and rise at an average rate of 20 Mm per day as they are aging; while the anchor depths of the short-lived spot groups

are located in the shallow layers since their first appearance. They also suggest that small-scale and mesoscale features would lie in the shallow layers just beneath the surface. Unfortunately, some authors infer the location of the flux source for internetwork elements to be below the tachocline, which has been estimated to be at a depth of 0.69 to 0.72 solar radii (Basu & Antia 1997). Although it could not completely exclude the possibility that the local creation of internetwork magnetic elements has something to do with the toroidal field generated by global dynamo in the deep layer, internetwork magnetic features clearly represent their local generation, and never show correlation with sunspot variation in a solar cycle as discussed above, also see Jin & Wang (2015).

On the other hand, Wang et al. (2012) estimate the depth of the internetwork field based on observations of internetwork bipolar flux emergence and theoretical consideration for the effectiveness of magnetic buoyancy. In the observations, a few internetwork ephemeral regions show interesting ‘magnetic float’ behavior. These authors suggest that the internetwork magnetic field is located at a somewhat shallow depth, approximately 1000 km below the surface, which is much shallower than that suggested by magnetic convection simulation (see Cheung et al. 2008; Toriumi & Yokoyama 2010).

Adopting the idea that the solar hidden flux has even more shallow depth and is truly small-scale in 3D, then we expect its impact on solar radiation and dynamics would be constrained and limited only on the solar surface, probably in the form of small scale disturbance. As in the surface layer where the plasma β is close to 1, the hidden magnetic flux would co-exist with the turbulent velocity field. Their collective behavior may provide a certain amount of magnetic energy which is continuously transmitted into the larger magnetic structures, e.g., internetwork and/or network field. The complicated dynamics and emergence observed on internetwork scale, for example the rapid flux appearance and disappearance, seem to manifest some of the disturbance made by the hidden flux on the observable scale. We might speculate a continued transmission of magnetic turbulence on internetwork scale into further large scales, which may play an important role in solar wind acceleration and coronal heating (see Tu et al. 2005).

6 CONCLUDING REMARKS AND DISCUSSION

In this study, HMI and SOT/SP observations are consistently calibrated and combined into a unique database in the interval from April 2010 to October 2015. An auto-

matic feature detection procedure is applied to the combined magnetograms. More than 20 million magnetic features are identified. The detected magnetic features are grouped into categories of sunspot/pore, enhanced network, quiet network and internetwork, based on their magnetic flux, flux density, atmospheric correspondence and cyclic variations. We use the HMI magnetic observations to study the magnetic structures with larger scale, i.e., sunspots/pores, enhanced and quiet network, and adopt the SP observation to study the internetwork field. The flux from internetwork field is estimated by comparing SOT/SP and HMI magnetic observations. Refer to the comprehensive Table 3, which describes the typical behaviors for observed magnetic categories. The following results are revealed:

- (1) The total flux from these magnetic features reaches 5.9×10^{22} Mx during solar minimum and 2.4×10^{23} Mx in solar maximum of solar cycle 24. The sunspot/pore contributes 29% of the total flux in the solar maximum, while the flux variation results from the area change, and their flux density keeps constant with a value of about 150 G.
- (2) The flux and area variations of enhanced network follow the sunspot cycle, and its flux contribution is about 18% during the solar minimum and about 50% in the solar maximum, which accounts for most flux in the solar surface during solar maximum.
- (3) The flux of quiet networks shows the anti-phase variation with sunspot cycle, which results from the area change, and quiet network contributes about 21% of flux to the surface magnetogram during the solar minimum and 9% of flux in solar maximum.
- (4) As had been revealed previously, the internetwork field has an important contribution to solar surface magnetism (Wang et al. 1995; Lites 2002; Zhou et al. 2013). In the solar minimum of solar cycle 24, internetwork field accounts for most flux on the solar surface, exceeding 55%, and the flux contribution from the internetwork is obviously more than that of the sunspot/pore, even in the solar maximum.

Below the detectability of SOT/SP, we have no idea what the types of magnetic structures would be. Their spatial scale should be smaller than the spatial resolution of SOT/SP, so that the flux of each undetectable magnetic structure should be smaller than 10^{16} Mx. If all magnetic structures follow the same distribution - a power law, it means that the flux from these undetectable magnetic structures would be only in the order of magnitude of several

Table 3 Observed Categories Based on HMI and SOT/SP Magnetic Observations

Category	Definition	Flux on solar surface	Area occupation (%)	CC
Sunspot/pore	Structure flux $> 1.0 \times 10^{20}$ Mx Maximum magnetic field > 950 G	$[0 - 1.3] \times 10^{23}$ Mx	$[0 - 4.8]$	–
Enhanced network	Structure flux $> 7.0 \times 10^{18}$ Mx Maximum magnetic field > 100 G	$[0.7 - 9.9] \times 10^{22}$ Mx	$[1.2 - 9.9]$	0.81
Quiet network	Structure flux $> 1.7 \times 10^{17}$ Mx Structure area $> 1.2 \times 10^{16}$ cm ²	$[1.2 - 1.5] \times 10^{22}$ Mx	$[4.4 - 5.5]$	–0.21
Internetwork	Structure flux $> 1.0 \times 10^{16}$ Mx Structure area $> 1.1 \times 10^{15}$ cm ²	$\sim [3.6 - 4.2] \times 10^{22}$ Mx	$\sim [14.6 - 16.6]$	–
Hidden region	Structure flux $\leq 1.0 \times 10^{16}$ Mx	$\sim [5.4 - 6.0] \times 10^{21}$ Mx	$\sim [68.6 - 79.0]$	–

Notes: The flux from hidden region is estimated by following Parnell et al. (2009). CC means the correlation coefficient between magnetic flux variation and sunspot cycle.

10^{21} Mx– 10^{22} Mx, although they occupy an area exceeding 65% of the solar surface.

It is interesting to note that sunspot/pore flux variation results from the area change, and its flux density does not show a clearly increasing or decreasing trend in this interval. Moreover, the internetwork flux variation comes from its area change too, but its flux density remains unchanged (Jin & Wang 2015; Lites et al. 2014). With state-of-the-art observations and careful magnetic feature detection, we are able to conclude that either solar mean-field dynamo or local small-scale dynamo is contained to maintain invariant magnetic flux density in producing magnetic fields. Observationally, network structures come from several sources: the fragmentation of decaying sunspots and/or pores, flux emergence in the form of ephemeral regions, coalescence of internetwork flux and products of interaction among different sources of magnetic flux. Variation in the enhanced network follows the sunspot cycle, but it has obviously more flux than sunspot/pore. More interestingly, both the area and flux density of the enhanced network increase during solar active condition, and the quiet network displays decreasing area and somewhat increasing flux density of 6% in solar maximum. These results constrain our consideration of its origin and evolution. Enhanced network represents an important aspect of solar activity, and comes from decayed or diffused sunspots/pores. It is a component of the solar mean-field dynamo. The magnetic flux diffusion seems to take longer in the enhanced network stage compared to the rapid decay of sunspot/pore features, and more flux is added into the appearance of the enhanced network by the decayed sunspot/pore field in terms of its duration as the enhanced network in the Sun’s active phase. This might explain the increase in area and flux density in the enhanced network. On the other hand, we guess that of the quiet network

suffers more from the interaction between the mean-field and the small-scale dynamos. It is a component of small-scale local dynamo, but partly comes from diffused enhanced network. Small-scale flux emergence in internetwork bipoles must have played a role in creating the quiet network field. Its area is suppressed by sunspot/pore and enhanced network fields, while flux density slightly increases in the solar active phase.

The flux participation studied in this work only refers to the solar surface magnetism. In fact each component in surface magnetism not only has difference in surface spatial scale, but also in vertical extension. From internetwork to quiet and enhanced network magnetic features, to sunspot/pore features, they have very different atmospheric extensions and anchor in different depths (Sivaraman & Gokhale 2004). In terms of magnetic energy, they have different contributions and even different manifestations. Sunspot/pore features anchor deeply and extend to the corona, and they seem to channel energy from the solar interior to the atmosphere (see Wang et al. 1997); while the internetwork structures offer continuous disturbance to larger magnetic structures, possibly through magnetic reconnection. So far, we do not have accurate knowledge about the roles of each magnetism component in solar activity and coronal heating. We expect that the huge amount of surface magnetic flux and their rapid appearance and disappearance from tiny internetwork fields hold the key to understanding coronal heating and solar wind acceleration.

Acknowledgements The authors are grateful to the team members who have made great contributions to the *SDO* mission and *Hinode* mission. *SDO* is a mission of NASA’s Living With a Star program. *Hinode* is a Japanese mission developed and launched by ISAS/JAXA, with NAOJ as domestic partner and NASA and STFC (UK) as inter-

national partners. Sunspot data are from the World Data Center SILSO, Royal Observatory of Belgium, Brussels. The work is supported by the National Natural Science Foundation of China (Grant Nos. 11373004, 11573038 and 11533008).

References

- Basu, S., & Antia, H. M. 1997, *MNRAS*, 287, 189
- Carlsson, M., Hansteen, V. H., Gudiksen, B. V., Leenaarts, J., & De Pontieu, B. 2016, *A&A*, 585, A4
- Cheung, M. C. M., Schüssler, M., Tarbell, T. D., & Title, A. M. 2008, *ApJ*, 687, 1373
- Gaizauskas, V. 1979, *JRASC*, 73, 299
- Gošić, M., Bellot Rubio, L. R., Orozco Suárez, D., et al. 2014, *ApJ*, 797, 49
- Hagenaar, H. J. 2001, *ApJ*, 555, 448
- Harvey, K. L., & Martin, S. F. 1973, *Sol. Phys.*, 32, 389
- Hudson, H. S. 1991, *Sol. Phys.*, 133, 357
- Ichimoto, K., Lites, B., Elmore, D., et al. 2008, *Sol. Phys.*, 249, 233
- Javaraiah, J., & Gokhale, M. H. 1997, *A&A*, 327, 795
- Jin, C. L., Wang, J. X., Song, Q., & Zhao, H. 2011, *ApJ*, 731, 37
- Jin, C., & Wang, J. 2011, *ApJ*, 732, 4
- Jin, C., & Wang, J. 2015, *ApJ*, 806, 174
- Lites, B. W. 2002, *ApJ*, 573, 431
- Lites, B. W., Kubo, M., Socas-Navarro, H., et al. 2008, *ApJ*, 672, 1237
- Lites, B. W., Centeno, R., & McIntosh, S. W. 2014, *PASJ*, 66, S4
- Liu, Y., Zhao, X., & Hoeksema, J. T. 2004, *Sol. Phys.*, 219, 39
- Marsh, K. A. 1977, *Sol. Phys.*, 52, 343
- Meunier, N., Solanki, S. K., & Livingston, W. C. 1998, *A&A*, 331, 771
- Moffatt, H. K. 1978, *Magnetic Field Generation in Electrically Conducting Fluids* (Cambridge: Cambridge Univ. Press)
- Parnell, C. E., DeForest, C. E., Hagenaar, H. J., et al. 2009, *ApJ*, 698, 75
- Parnell, C. E., & Jupp, P. E. 2000, *ApJ*, 529, 554
- Scherrer, P. H., Schou, J., Bush, R. I., et al. 2012, *Sol. Phys.*, 275, 207
- Schou, J., Scherrer, P. H., Bush, R. I., et al. 2012, *Sol. Phys.*, 275, 229
- Schrijver, C. J., & Harvey, K. L. 1994, *Sol. Phys.*, 150, 1
- Schrijver, C. J., Title, A. M., van Ballegoijen, A. A., Hagenaar, H. J., & Shine, R. A. 1997, *ApJ*, 487, 424
- Shimizu, T., Nagata, S., Tsuneta, S., et al. 2008, *Sol. Phys.*, 249, 221
- Sivaraman, K. R., & Gokhale, M. H. 2004, *Sol. Phys.*, 221, 209
- Suematsu, Y., Tsuneta, S., Ichimoto, K., et al. 2008, *Sol. Phys.*, 249, 197
- Toriumi, S., & Yokoyama, T. 2010, *ApJ*, 714, 505
- Tsuneta, S., Ichimoto, K., Katsukawa, Y., et al. 2008, *Sol. Phys.*, 249, 167
- Tu, C.-Y., Zhou, C., Marsch, E., et al. 2005, *Science*, 308, 519
- Van Kampen, N. G. 1976, *Phys. Rep.*, 24, 171
- Wang, J., Wang, H., Tang, F., Lee, J. W., & Zirin, H. 1995, *Sol. Phys.*, 160, 277
- Wang, J., Shibata, K., Nitta, N., et al. 1997, *ApJ*, 478, L41
- Wang, J., Zhou, G., Jin, C., & Li, H. 2012, *Sol. Phys.*, 278, 299
- Zhang, J., Wang, Y., & Liu, Y. 2010, *ApJ*, 723, 1006
- Zhou, G., Wang, J., & Jin, C. 2013, *Sol. Phys.*, 283, 273
- Zirin, H. 1972, *Sol. Phys.*, 22, 34
- Zirin, H. 1987, *Sol. Phys.*, 110, 101